environmental microbiology

Environmental Microbiology (2017) **19**(6), 2151–2163 doi:10.1111/1462-2920.13677

Ultrastructure of ellipsoidal magnetotactic multicellular prokaryotes depicts their complex assemblage and cellular polarity in the context of magnetotaxis

Pedro Leão,[1] Yi-Ran Chen,[2,3] Fernanda Abreu,[1] Mingling Wang,[2] Wei-Jia Zhang,[3,4] Ke Zhou,[2] Tian Xiao,[2,3] Long-Fei Wu[3,5]* and Ulysses Lins[1]**

[1]*Instituto de Microbiologia Paulo de Góes, Universidade Federal do Rio de Janeiro, Rio de Janeiro, RJ 21941-902, Brazil.*

[2]*Key Laboratory of Marine Ecology and Environmental Sciences, Institute of Oceanology, Chinese Academy of Sciences, Qingdao, China.*

[3]*CNRS, Laboratoire International Associé de la Bio-Minéralisation et Nano-Structures (LIA-BioMNSL), Marseille, France.*

[4]*Laboratory of Deep Sea Microbial Cell Biology, Institute of Deep Sea Science and Engineering, Chinese Academy of Sciences, Sanya 572000, China.*

[5]*Aix Marseille Univ, CNRS, LCB, Marseille, France.*

Summary

Magnetotactic multicellular prokaryotes (MMPs) consist of unique microorganisms formed by genetically identical Gram-negative bacterial that live as a single individual capable of producing magnetic nanoparticles called magnetosomes. Two distinct morphotypes of MMPs are known: spherical MMPs (sMMPs) and ellipsoidal MMPs (eMMPs). sMMPs have been extensively characterized, but less information exists for eMMPs. Here, we report the ultrastructure and organization as well as gene clusters responsible for magnetosome and flagella biosynthesis in the magnetite magnetosome producer eMMP *Candidatus* Magnetananas rongchenensis. Transmission electron microscopy and focused ion beam scanning electron microscopy (FIB-SEM) 3D reconstruction reveal that cells with a conspicuous core-periphery polarity were organized around a central space. Magnetosomes were organized in multiple chains aligned along the periphery of each cell. In the partially sequenced genome, magnetite-related *mamAB* gene and *mad* gene clusters were identified. Two cell morphologies were detected: irregular elliptical conical 'frustum-like' (IECF) cells and H-shaped cells. IECF cells merge to form H-shaped cells indicating a more complex structure and possibly a distinct evolutionary position of eMMPs when compared with sMMPs considering multicellularity.

Received 21 November, 2016; revised 11 January, 2017; accepted 18 January, 2017. For correspondence. *E-mail: wu@imm.cnrs.fr; Tel. 33-4 9116 4157; Fax 33-4 9171 8914. **E-mail: ulins@micro.ufrj.br; Tel. +55-21 3938-6738; Fax +55-21 2560-2580.

© 2017 Society for Applied Microbiology and John Wiley & Sons Ltd

Introduction

Magnetotactic bacteria (MTB) comprise a morphologically and phylogenetic diverse group of microorganisms capable of producing nano-sized, membrane-bound magnetic organelles called magnetosomes (Bazylinski and Frankel, 2004). Magnetosomes allow the passive orientation to the geomagnetic field, which is associated with flagellar movement to find the optimal conditions to survive and grow in stratified aquatic environments in a phenomenon called magnetotaxis (Frankel *et al.*, 1997). MTB morphotypes include cocci, vibrio, rods and the conspicuous magnetotactic multicellular prokaryotes (MMPs). MMPs are mostly uncultured, and culture-independent techniques based on 16S rRNA coding gene sequencing are used to determine the phylogeny. Microscopy is used to characterize the magnetic behaviour and morphological features of these microorganisms. Enrichment cultures have been maintained in the laboratory for a single strain of MMP named *Candidatus* Magnetoglobus multicellularis (Abreu *et al.*, 2007), but the microorganisms lost their motility and their capacity of producing magnetosomes (Abreu *et al.*, 2014).

Two distinct morphotypes of MMPs have been described so far, spherical MMPs (sMMPs; Keim *et al.*, 2004a) and ellipsoidal MMPs (eMMPs; Lefèvre *et al.*, 2007; Zhou *et al.*, 2012). sMMPs are distributed globally (Farina *et al.*, 1983; Rodgers *et al.*, 1990; Keim *et al.*, 2004b; Abreu *et al.*, 2007; Lins *et al.*, 2007; Wenter *et al.*, 2009; Zhou *et al.*, 2013; Zhang *et al.*, 2014), whereas eMMPs have only been reported from: the Yellow Sea, China (Zhou *et al.*, 2012; Chen *et al.*, 2015); the Mediterranean Sea, France (Lefèvre *et al.*, 2007; Chen *et al.*, 2016); and the South China Sea (Chen *et al.*, 2016). Phylogenetic

analysis based on 16S rRNA coding gene showed that both sMMPs and eMMPs are affiliated with the *Deltaproteobacteria* class of Bacteria. The sMMPs consist of several clades, possibly forming numerous species (Farina *et al*., 1983; Abreu *et al*., 2007; Simmons and Edwards, 2007; Wenter *et al*., 2009; Zhou *et al*., 2013; Zhang *et al*., 2014). eMMPs are closely related to sMMPs, but appear to belong to different genera (Chen *et al*., 2015; Chen *et al*., 2016). Morphologically, sMMPs and eMMPs are assemblages of bacterial cells that swim as a unit and respond to a magnetic field because of the thousands of magnetosomes organized in chains within their cells (Keim *et al*., 2004b; Lins *et al*., 2007; Wenter *et al*., 2009). sMMPs produce pleomorphic greigite (Fe_3S_4) magnetosomes, bullet-shaped magnetite (Fe_3O_4) magnetosomes (Lins *et al*., 2007), tooth-shaped greigite magnetosomes (Posfai *et al*., 1998) or both types (Lins *et al*., 2007; Zhang *et al*., 2014), whereas most eMMPs produce only bullet-shaped magnetite magnetosomes, except for *Ca*. Magnetananas rongchenensis, which produces both bullet-shaped and parallelipedal magnetite magnetosomes (Chen *et al*., 2015; Chen *et al*., 2016).

In sMMPs, cells within the organism are positioned side by side with flagella distributed along the cell surface in direct contact with the external environment and an internal non-flagellated cellular portion facing an internal acellular compartment (Keim *et al*., 2004a). The multicellular nature of sMMPs is emphasized by the observation that individual cells are not viable once disaggregated (Abreu *et al*., 2006) and its exclusive multicellular life cycle (Keim *et al*., 2004b). Winklhofer *et al*. (2007) showed that the cell arrangement and magnetosome disposition in the sMMP *Ca*. M. multicellularis has a high degree of magnetic optimization that cannot be observed in a random aggregation of bacterial cells. 3D reconstruction based on serial section transmission electron microscopy showed that magnetosome chains within *Ca*. M. multicellularis cells are positioned close to the cell surface facing the external environment and are arranged mostly parallel to each other (Abreu *et al*., 2013). The partial genomic sequencing of *Ca*. M. multicellularis showed that the greigite and magnetite syntheses have common ancestry and that the magnetosome genes *mam-A-B-E-K-M-O-P-Q* and *-T* are conserved in both processes (Abreu *et al*., 2011). eMMPs are composed of approximately 40 to 86 cells organized in a 10 x 8 μm assemblage (Zhou *et al*., 2012; Chen *et al*., 2015; Chen *et al*., 2016) containing thousands of magnetosomes organized in chains. Fluorescent lipid staining showed that an outer layer (Zhou *et al*., 2012) envelops the whole organism. Light and scanning electron microscopy observations confirmed that eMMPs exhibit a multicellular life cycle, with eMMP division occurring on either the long or the short axis (Zhou *et al*., 2012; Chen *et al*., 2015).

The morphologies of both sMMPs and eMMPs are considered unique among prokaryotes, but the morphology of sMMPs has been better characterized (Abreu *et al*., 2013). The cellular internal ultrastructure, detailed multicellular organization, and magnetosome genes have only been studied in sMMPs. Here, we used transmission electron microscopy and focused ion beam scanning electron microscopy imaging associated with 3D reconstruction to characterize the ultrastructure and organization of the cells within the eMMP *Ca*. M. rongchenensis and the magnetosome arrangements within each cell and in the whole organism. Partial genomic data are also provided regarding magnetosome and flagellar genes. These results provide additional data for a better understanding of bacterial multicellularity and magnetotaxis.

Results

Cell organization and ultrastructure

The ultrathin-section TEM of *Ca*. M. rongchenensis showed that cells are organized side by side in a regular pattern assembled into an ellipsoidal entity with a core-periphery polarity (Fig. 1A). Bullet-shaped magnetosomes were observed in the cytoplasm of the cells closer to the outer surface of the assemblage (Fig. 1A and D; white arrows). Electron-dense filaments were observed perpendicular to the cell symmetry axis (Fig. 1A; black arrows). These filaments resembled the so-called striated structures in *Ca*. M. multicellularis (Abreu *et al*., 2013). A single filament was usually observed for each cell and was located close to the cell membrane in contact with the external environment. A round to ovoid region consisting of a fibrillar network structure was located close to the centre of each cell, possibly representing the nucleoid (Fig. 1A; N). Most cells seemed to be triangle-shaped, with a larger surface in contact with the external environment and a smaller surface facing an internal acellular region, similar to sMMPs (Keim *et al*., 2004a). The surfaces of two adjacent cells were juxtaposed. A zig-zag pattern was commonly observed, which is typical of chemically fixed Gram-negative bacterial cell walls and membranes. Nevertheless, no special adhesive structures were observed between cells. An internal compartment delimited by the cells was present at the centre of the MMP assemblage (Fig. 1B). The cellular surface in contact with the internal compartment consisted of a meshwork of thin fibrils distributed around the compartment and seemed to define an acellular space within the assemblage (Fig. 1B). In this space, numerous round vesicles were observed (Fig. 1C; black arrowheads). The membranes of some vesicles remain connected with the cellular membrane (Fig. 1C). In the cytoplasm, electron-lucent round granules (Fig. 1A, B and G), magnetosomes (Fig. 1D) and undescribed tabular structures were observed (Fig. 1D; T). Highly abundant tabular structures (Fig. 1D,

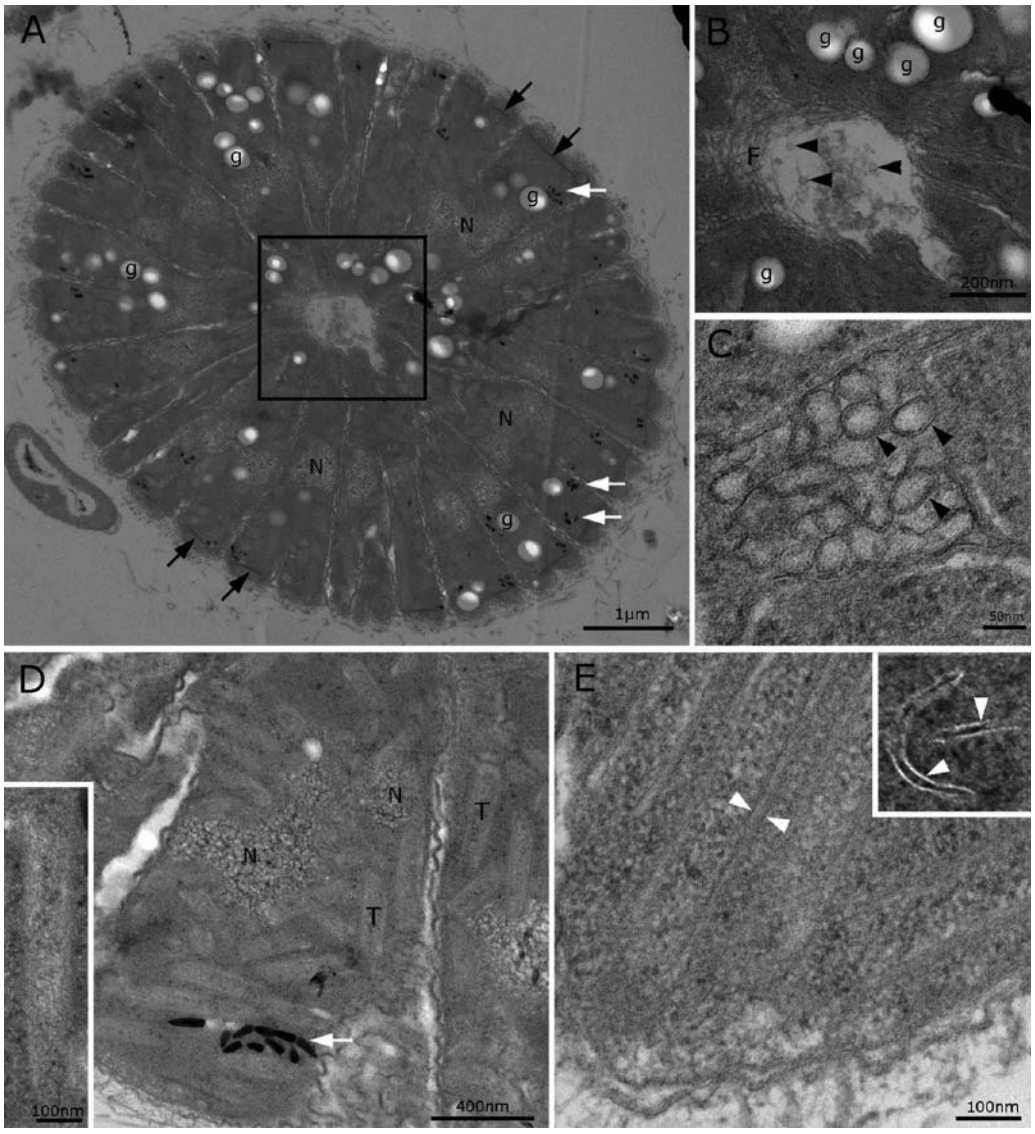

Fig. 1. Cell ultrastructure and organization in *Ca*. Magnetananas rongchenensis.
A. Ultrathin section TEM image showing the organization of cells with a large area in contact with the environment and a small acellular region in the middle (square). Note the filamentous structures (black arrows) and magnetosomes (white arrows). Inside each cell, there is a translucent region corresponding to the nucleoid (N).
B. High magnification of selected area (square) in A showing fibrillary (F) material and vesicles (black arrowheads). Granules (g) are present inside cells.
C. High-magnification image of double-membrane vesicles (black arrowheads) filling the space between adjacent cells.
D. Cylindrical translucent structures (T) in cell cytoplasm; inset shows a high-magnification image of the structure. Nucleoids (N) and magnetosomes (white arrow) can be observed.
E. Tubular membrane profiles (white arrowheads) in the cytoplasm. Inset: cytochemical staining with tannic acid showing electron-dense material inside the membranous structures (white arrowheads).

inset) were more electron-lucent than the surrounding cytoplasm and were 89.6 nm ± 8.7 nm wide ($n = 10$) and 329.2 nm ± 58.9 nm long ($n = 10$). Numerous membrane profiles were observed in the cytoplasm (Fig. 1E). These profiles consisted of tubular or flat structures (Fig. 1E, white arrowheads). Cytochemical staining with tannic acid showed an electron-dense material inside the membranous structures (Fig. 1E inset, white arrowheads), possibly composed of proteinaceous material.

Cell surface and motility

The scanning electron microscopy of *Ca*. M. rongchenensis confirmed the presence of numerous cells organized in

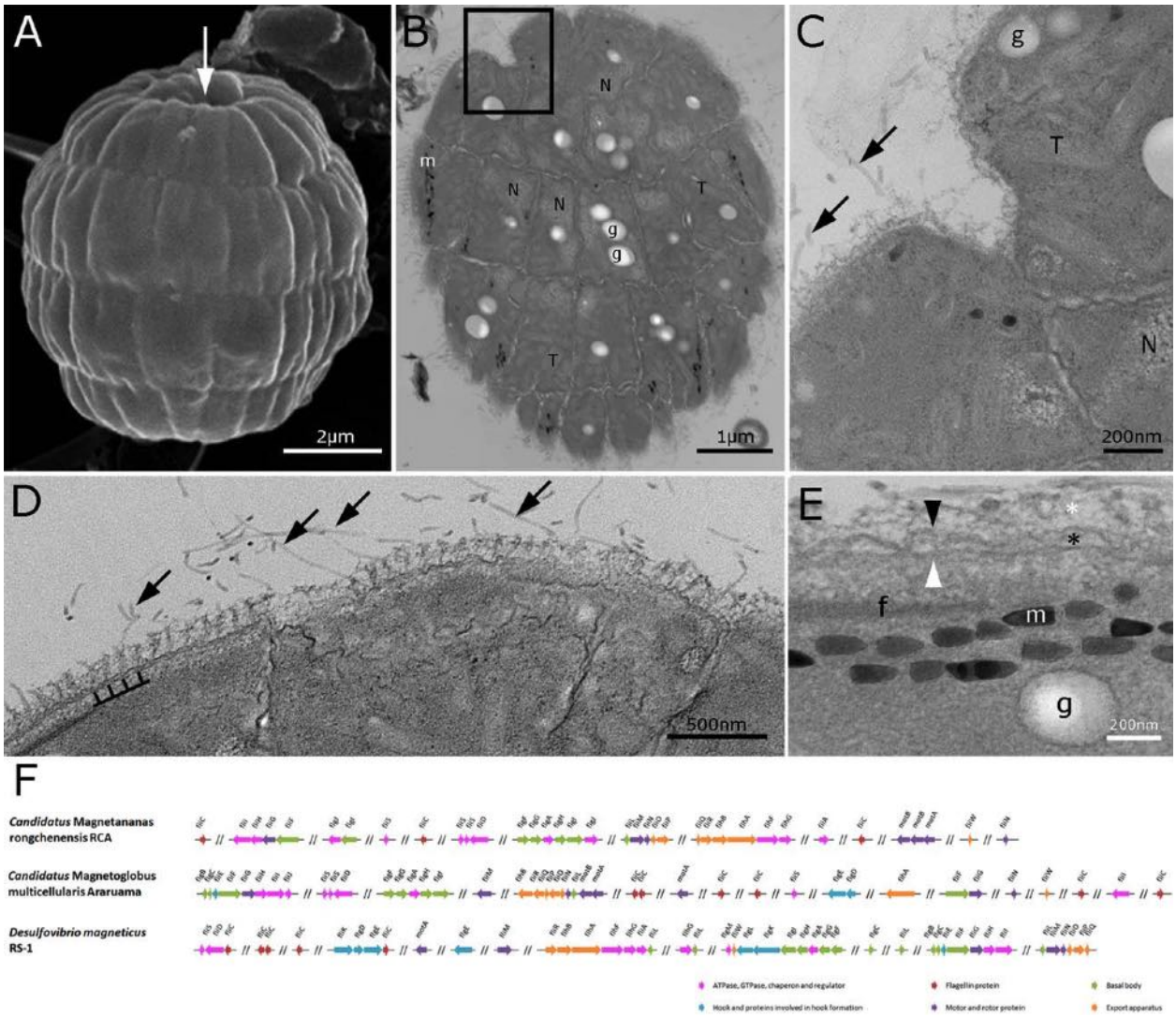

Fig. 2. Cell surface, flagellar apparatus and flagellar genes in *Ca*. Magnetananas rongchenensis.
A. SEM showing a small mouth-like structure on the pole of the assemblage representing a non-cellular region of the surface.
B. Ultrathin section showing a small portion of that mouth-like structure (square).
C. High magnification of selected area (square) in B showing the mouth-like indentation. Black arrows show flagellar filaments.
D. Regular distribution (row of thin black lines) of flagellar filaments on the cell surface; black arrows show broken flagellar filaments.
E. Complex surface structure of *Ca*. M. rongchenensis showing the cytoplasmic membrane (white arrowhead), outer membrane (black arrowhead), periplasmic space (black asterisk) and capsular material (white asterisk), filamentous structure (f) and magnetosomes (m). A granule (g) can be observed.
F. Organization of flagella genes of *Ca*. M. rongchenensis, the sMMP *Ca*. M. multicellularis and the unicellular magnetite-producing *D. magneticus* RS-1 associated also with *Deltaproteobacteria*. [Color figure can be viewed at wileyonlinelibrary.com]

a highly complex assemblage (Fig. 2A). At the poles, a specialized region corresponding to an indentation of the eMMP surface was observed (Fig. 2A, white arrow). The ultrathin section TEM of this area revealed the presence of a region without contact between adjacent cells (Fig. 2B). High magnification showed that the intercellular connections between cells were not present in this area (Fig. 2C). Numerous filamentous structures with the size and structure consistent with bacterial flagellar filaments already observed in different bacteria (Chen *et al*., 2011), including sMMPs (Silva *et al*., 2007) were observed at the cell surface facing the external environment (Fig. 2D, black arrows). The filaments consisted of 18.8 nm $\pm$ 1.75 nm ($n = 39$) tubes of variable length, probably because the filaments were broken during the processing for electron microscopy. Nevertheless, the flagellar bases were preserved. It is observed in some areas that the flagella were distributed regularly on the cell surface at 56.9 nm $\pm$ 2.5 nm

($n = 24$) intervals (Fig. 2D). A complex surface profile with a Gram-negative cell wall consisting of a plasma membrane (Fig. 2E, white arrowhead), periplasmic space (Fig. 2E, black asterisk), an external membrane (Fig. 2E, black arrowhead) and capsular material (Fig. 2E, white asterisk) was observed (Fig. 2E). Electron-dense filamentous structures near the cell portion in contact with the external environment (Fig. 2E and F) were associated with bullet-shaped magnetosomes usually found in chains (Fig. 2E; m). Several granules were occasionally detected in the cytoplasm close to the surface (Fig. 2E; g).

Regarding motility, in the currently available partial genome of *Ca*. M. rongchenensis, a total of 36 genes involved in flagellar synthesis were identified in 14 contigs, with 29 genes forming 7 clusters and the other 7 genes located on separate contigs (Fig. 2F). Compared with the thoroughly studied flagellar apparatus of *E. coli*, 11 genes encoding chaperones or proteins involved in the basal body and hook synthesis were missing from the partially sequenced genome. Most of the flagellar synthesis related genes have a single copy, while others such as the rotation switcher *fliN* and motor *motB* have two copies, and the flagellin *fliC* and chaperone *fliS* have three copies. For the genes having multiple copies, the identity between homologues varied from 40% to 50%, except for *fli*C gene. Tens of thousands of copies of single or multiple flagellins constitute the flagellar filament. The N- and C-termini of FliC are highly conserved, while the length and sequence of the middle region that should be exposed at the surface of the filament varied considerably between species. Two of the three *fliC* genes identified in *Ca*. M. rongchenensis have a similar length of 2,000 bp, significantly longer than that of the third copy of 800 bp. Such character is conserved in magnetotactic bacteria affiliated with *Deltaproteobacteria*. For *Ca*. M. multicellularis, five *fli*C coding genes are approximately 1,500 bp, and the sixth is less than 800 bp, and for *D. magneticus* RS-1, three *fli*C genes have a gene length double that of the other two genes. Genes encoding FlhF and FlhG, which are responsible for flagellar number and insertion (Altegoer *et al*., 2014), were identified in the draft genome of the eMMP. FlhF is a signal recognition particle-type GTPase. Its homologues Ffh and FtsY are known to be involved in the targeting and insertion of membrane proteins into the translocation apparatus. FlhG is a MinD-like ATPase. It is speculated that FlhG may stimulate GTP hydrolysis of FlhF and regulate the localization of the flagellar MS-ring, which is first assembled during the synthesis of the flagellar apparatus (Schuhmacher *et al*., 2015). According to TBLASTN analysis, the closest related FlhF homologues were those from two sMMPs (*Ca*. Magnetomorum strain HK-1 and *Ca*. M. multicellularis) with an identity of approximately 60%, followed by two from *Desulfatibacillum* with 47% identities, and the other best hits were lower than 40%. Interestingly, the identity with *flhF* from the unicellular *D. magneticus* RS-1 is only 24%, although both strains belong to *Deltaproteobacteria*. Similar as for *flhF*, *flhG* is more conserved, sharing an approximately 67% identity with homologues from the two sMMPs and 44.44% with those from *D. magneticus* RS-1. It is plausible that the highly conserved features of FlhF and FlhG might be responsible for regularly positioning the flagella only at the outer surface of the MMP cells.

Magnetosome organization and genomic analysis of magnetotaxis-related genes

Magnetosomes were mostly observed closer to the cell periphery, forming linear chains (Fig. 3A). A clear membrane could be observed surrounding each magnetosome (Fig. 3A inset, arrowheads). Two types of magnetosome arrangement in chains were observed. In most cases, the magnetosomes were oriented in the same head-tail direction in the chain (Fig. 3B) and, more rarely, some neighbouring magnetosomes were aligned with an opposite tail-tail orientation, (Fig. 3C). To better understand the spatial relationships between magnetosomes in a chain, we have used scanning transmission electron microscopy tomography with a high-angle annular dark-field detector. Figure 3D shows two voxel projections with a 20° difference in their tomographic reconstructions, revealing the three-dimensional structure of the magnetosomes in a chain. It can be observed that the magnetosomes are not co-planar, showing a variation in the inclination within the chains.

We have identified a 42,381-bp magnetosome island (MAI) on a 44,522-bp contig from the draft genome of *Ca*. M. rongchenensis (for accession numbers, see Supporting Information Table S1). It is composed of 13 *mam* genes (for 'magnetosome membrane') and 19 *mad* genes (for 'magnetosome-associated *Deltaproteobacteria*') and has a similar gene order to those of the magnetite-producing gene clusters found in magnetotactic *Deltaproteobacteria*, including one sMMP (*Ca*. Magnetomorum strain HK-1) and two unicellular MTBs (*Ca*. *Desulfamplus magnetomortis* BW-1 and *Desulfovibrio magneticus* RS-1) (Fig. 3E; Supporting Information Table S1). It has been reported that typical MAI of *Deltaproteobacteria* consists of two or three gene clusters. The first one is the *mad* gene cluster that is specific to *Deltaproteobacteria* and some *Nitrospirae* (Blue colour in Fig. 1, Lefèvre *et al*., 2013; Kolinko *et al*., 2014; Lin *et al*., 2014). The second one is a *mamAB*-like operon that is conserved in all magnetite-producing magnetotactic bacteria and is putatively involved in magnetite biomineralization (Yellow colour in Fig. 8, Lefèvre *et al*., 2013; Ji *et al*., 2014; Kolinko *et al*., 2014). The third one is also a *mam* gene cluster, which is closely related to the greigite-producing magnetotactic bacteria and remotely related to the *mamAB* gene clusters of

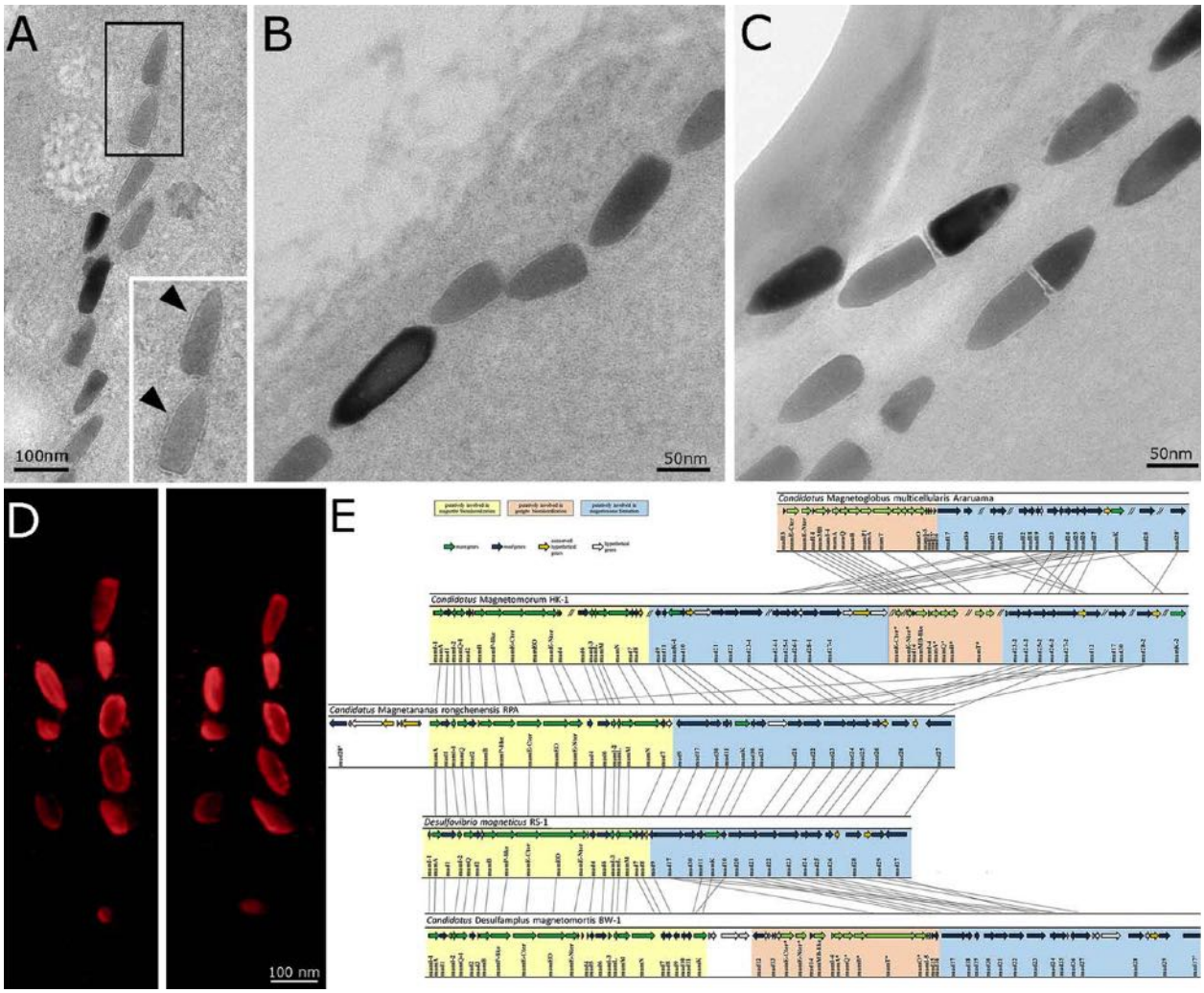

Fig. 3. Magnetosome organization and genomic related genes in *Ca*. Magnetananas rongchenensis.
A. Bullet-shaped magnetosomes in *Ca*. M. rongchenensis cytoplasm. Inset shows a TEM image of a stained thin section of magnetosomes within cells of *Ca*. M. rongchenensis. Note the presence of a layer surrounding both anisotropic magnetite crystals, suggestive of the presence of a magnetosome membrane (arrowheads).
B. Single chain of magnetosomes close to the cell surface.
C. Bullet-shaped magnetosomes with opposite alignments in the same chain.
D. STEM tomographic reconstruction showing two magnetosome chains rotated by 20 degrees around the major axis of the chains. Note that the magnetosomes are not coplanar in the chain.
E. Organization of magnetotaxis-related genes, *mam* and *mad* clusters, of *Ca*. M. rongchenensis and other selected MTBs, including the MMPs in *Deltaproteobacteria*. [Color figure can be viewed at wileyonlinelibrary.com]

magnetite-producing MTB and is putatively involved in greigite biomineralization (Orange colour in Fig. 8, Abreu *et al*., 2011; Lefèvre *et al*., 2013; Kolinko *et al*., 2014). The MAI of *Ca*. M. rongchenensis contains only the magnetite-producing *mamAB*-cluster and the *mad* gene cluster, which are highly conserved and display similar gene compositions and order compared with the MAI of the magnetite-producing unicellular *D. magneticus* RS-1 (Fig. 3E). The greigite-producing *mam* gene cluster, which was found in the two sMMP genomes (Abreu *et al*., 2011; Kolinko *et al*., 2014), was not found in the partial genomic sequence of *Ca*. M. rongchenensis (Fig. 3E). It might be on a position of the genome of *Ca*. M. rongchenensis that has not been sequenced yet.

Multicellular morphology and magnetosome distribution based on FIB-SEM 3D reconstruction

The direct TEM imaging of the magnetosome organization in air-dried whole cells can be misleading because of shrinking artefacts, which can seriously distort cell positioning, thickness and magnetosome arrangement. Ultra-

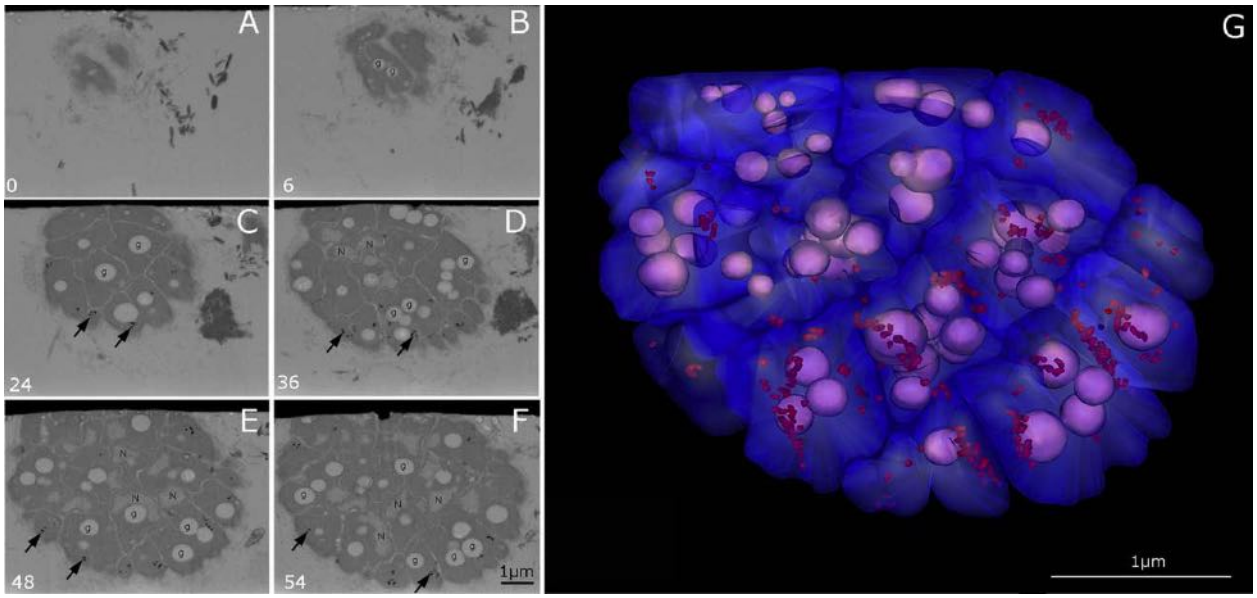

Fig. 4. Magnetosome distribution in *Ca*. Magnetananas rongchenensis based on FIB-SEM image reconstruction.
A–F. Series of sections of *Ca*. M. rongchenensis, where the number in the low left represents the section number in the image series.
G. Magnetosome chains (arrows) are organized parallel to each other and are distributed on the periphery of the cells, forming aligned chains along the long axis of the eMMP assemblage. Lipid granules (g) and nucleoids (N) can be observed. Cell membranes are shown in blue, magnetosomes in red and lipid granules in pink. [Color figure can be viewed at wileyonlinelibrary.com]

thin sectioning is in this respect a superior approach, but the three-dimensional relationships between cell components are then lost. FIB sectioning associated with 3D reconstruction is an alternative that overcomes these limitations. Figure 4A–F are images of a partial FIB-SEM image series of a single eMMP. Magnetosomes (Fig. 4, arrows), a nucleoid (Fig. 4, N) and granules (Fig. 4, g) could be observed. The electron-lucent granules appear to follow the cell shape and can be observed as round structures inside cells (Fig. 4, g). The 3D reconstruction of the same image series (Fig. 4G) shows that magnetosomes are organized in multiple chains arranged along the long axis of the MMP assemblage. The magnetosomes were positioned close to the cell surface next to the periphery in *Ca*. M. rongchenensis cells (Fig. 4G, red). The chains in each cell are oriented in the same direction in relation to other cells in the whole microorganism, which guarantees that the chain of magnetosomes in one cell maintains the same direction in the adjacent cells, making all the chains parallel to each other. This optimized arrangement has been observed in sMMPs (Winklhofer *et al*., 2007), which are also organized as a unit to efficiently orient the whole organisms in the geomagnetic field.

Two different cell morphologies with small variations were observed in *Ca*. M. rongchenensis based on FIB-SEM imaging (Fig. 5). In the first morphological type (Fig 5A and B), cells are longer and maintain an irregular elliptical conical 'frustum-like' shape (IECF-shaped) to reach the centre of the whole microorganism. These cells are usually at the polar region of the MMP assemblage, and this shape is sometimes referred to as triangle-shaped (Chen *et al*., 2015). Figure 5B shows a side-view 3D reconstruction of the IECF-shaped cells. The second morphological type comprises the so-called H-shaped cells (Fig. 5C and D; Chen *et al*., 2015), which are mostly positioned in the middle rings of the eMMP. Figure 5D shows a side-view 3D reconstruction of the H-shaped cells. Serial imaging showed that most cells are first observed as IECF-shaped cells. Serial sectioning and imaging revealed that some IECF-shaped cells continuously show characteristics of a H-shaped. Reconstruction and modelling of the same series suggests that this merging of IECF-shaped cells into H-shaped cell could be either a form of cellular differentiation or a stage in cell division (Fig. 6).

Discussion

Most MTBs are unicellular with one or multiple chains of magnetosomes aligned along the major cell axis (Bazylinski and Frankel, 2004). One notable exception is the magnetotactic multicellular prokaryotes (MMPs), which consist of a highly complex assemblage of bacterial cells capable of a collective magnetotactic response. Understanding the spatial relationship between the cellular components in MMPs may provide the structural framework for the correct interpretation of the genomic data and its adaptive roles in the environment. Here, we studied the cell ultrastructure and magnetosome-related genes in the

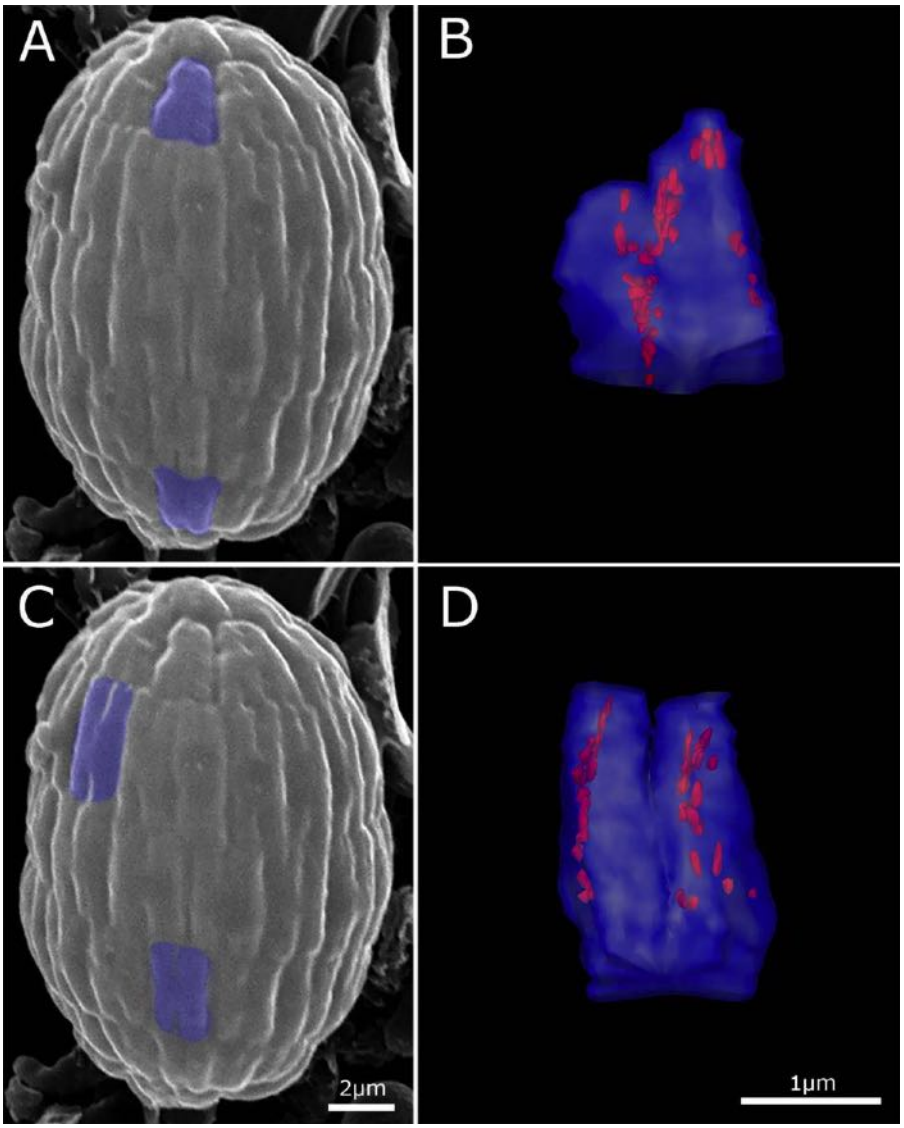

Fig. 5. Cell specialization in *Ca*. Magnetananas rongchenensis. Two morphological types of cells are observed, the irregular elliptic conical frustum (IECF)-shaped cells (A and B) and H-shaped cells (C and D).
A. Scanning electron microscopy image of Ca. M. rongchenensis highlighting two IECF cells.
B. Side view 3D reconstruction of an IECF-shaped cell.
C. Scanning electron microscopy image of Ca. M. rongchenensis highlighting H-shaped cells.
D. Side view 3D reconstruction of an H-shaped cell. Cell membranes are shown in blue, and magnetosomes are shown in red. [Color figure can be viewed at wileyonlinelibrary.com]

eMMP *Ca*. M. rongchenensis. The overall ultrastructure of *Ca*. M. rongchenensis cells is similar to that of sMMP cells with respect to their cell walls, flagella, magnetosome configuration in chains, presence of a nucleoid, and presence and position of peripheral filaments (striated structure) and granules. Abreu *et al*. (2013) described an extracellular carbohydrate layer loosely linked to the cell surface and between adjacent cells in sMMPs. This layer is possibly responsible for maintaining the formation of the cells, and the unique cell arrangement in the multicellular morphology could be determined by the individual cell variation in size and shape in the same MMP. In *Ca*. M. rongchenensis, capsular material was also observed, which is similar to the structure described for sMMPs. However, it appears to be thicker in the internal compartment.

Three types of granules are present in *Ca*. M. multicellularis: polyhydroxyalkanoate-like granules, non-PHA lipid granules, and phosphorus-rich granules (Silva *et al*., 2007). In *Ca*. M. rongchenensis, electron-lucent granules, probably composed of polyhydroxyalkanoate based on comparison with sMMP images, were observed. *Ca*. M. rongchenensis also has an acellular compartment in the middle of the organism where cells may communicate with each other using membrane vesicles, as suggested for *Ca*. M. multicellularis (Keim *et al*., 2004a). The membrane profiles observed in the cytoplasm of *Ca*. M. rongchenensis have been previously described in magnetotactic bacteria in the *Deltaproteobacteria* class (Byrne *et al*., 2010), but their function remain unknown. The electron-dense filaments observed close to the cell pole next to the surface of the eMMP seem to be common to all MMPs. These structures were denominated striated structures in *Ca*. M. multicellularis (Abreu *et al*., 2013). In *Ca*. M. rongchenensis, however, no striations were observed in the filament.

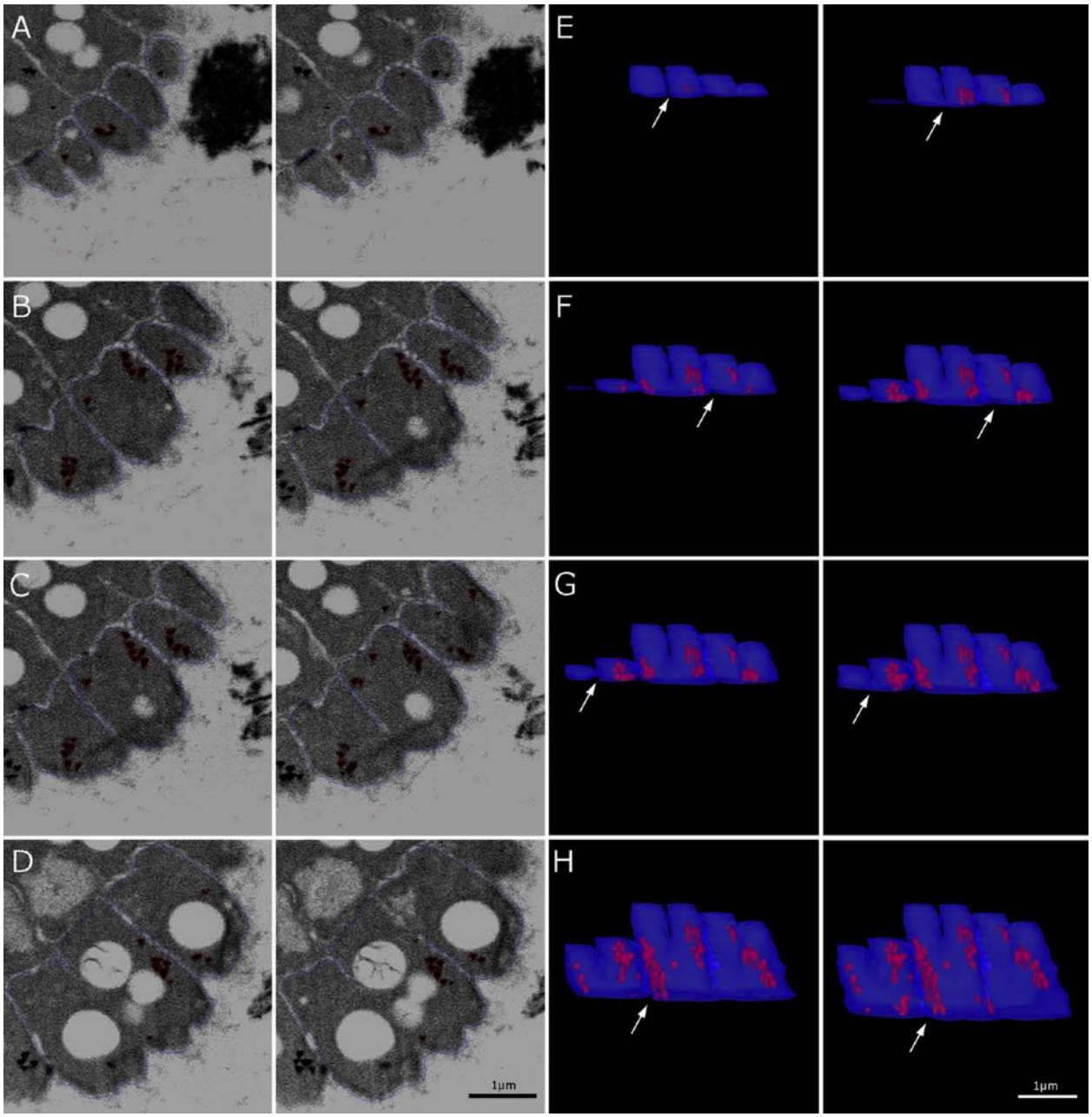

Fig. 6. *Ca*. Magnetananas rongchenensis cells merging to form H-shaped cells. FIB-SEM image series (A–D) and 3D reconstruction (E–H) of cells in a single eMMP.
A. Image series showing neighbour cells apart before merging; the image to the right shows the next section after they merge.
B–C. Subsequent images showing the same cells shown in A connected.
D. Subsequent images showing fully merged cells.
E–H. 3D side-view models of the cells shown in A–D series displayed at different depths within the eMMP assemblage. Arrows show connecting points between adjacent cells. Cell membranes are shown in blue, and magnetosomes in red. [Color figure can be viewed at wileyonlinelibrary.com]

The function of these structures remains unknown, but they resemble the chemoreceptors described in the *Bacteria* domain (Briegel and Auer, 2013). The undescribed tabular structures observed in the cytoplasm are unique to eMMPs, and their high abundance would suggest an important structural or functional role. These structures slightly resemble carboxysomes (Rae *et al*., 2013), but their typical polyhedral shape is not preserved, and we could not unequivocally determine the presence of a protein coat (Rae *et al*., 2013). Further genomic analysis could provide information regarding the presence of carboxysome coat proteins that can be expressed during

heterotrophic growth or the ability of eMMPs to produce carboxysomes and grow autotrophically (Bobik *et al*., 1999).

The motility and flagellar distribution on the cellular external surface seems to be identical in all MMPs. However, the flagellar insertion points appear to be regularly distributed in *Ca*. M. rongchenensis, which was not clearly observed in the sMMPs (Silva *et al*., 2007). Similar flagella-related genes have been observed in *Ca*. M. multicellularis. The presence of multiple copies of flagellin and its chaperone, one more set of a flagellar motor and motor switching protein, in addition to a full set of flagellar synthesis related genes might be a common feature to all MMPs. The high similarity of FlhF between eMMPs and sMMPs (*Ca*. Magnetomorum strain HK-1 and *Ca*. M. multicellularis) is remarkable. It is possible that MMPs use different mechanisms of positioning the flagella from those of unicellular magnetotactic bacteria. Arguably, multiple flagellar genes could also be used in the characterization of this group to reflect the multicellular life of MMPs.

The cell shape varies between eMMP and sMMPs. In *Ca*. M. rongchenensis, cells are IECF-shaped, also called triangular-shaped cells (Chen *et al*., 2015), or H-shaped. FIB-SEM 3D modelling and reconstruction showed that the IECF-shaped cells are usually observed at positions close to the poles of the assemblage, whereas the H-shaped cells are located closer to the equator. This morphological difference has been previously reported by Chen *et al*. (2015), and it suggests a possible differentiation among cells in eMMPs. 3D modelling and TEM images suggest that, unlike *Ca*. M. multicellularis (Abreu *et al*., 2013), not all cells would be in contact with the internal compartment of *Ca*. M. rongchenensis. Those cells that are not in contact are still highly organized within the elliptical microorganism and are not 'detached' cells. Often, vesicles are observed inside the acellular compartment and between adjacent cells, indicating that some vesicles translocate and can be involved in cellular communication, as suggested for sMMPs (Keim *et al*., 2004a). Prokaryote vesicle production has been reported and associated with cell-to-cell communication (Berleman and Auer, 2013). The vesicle ultrastructure profiles observed in this study are compatible with a membrane bilayer; the diameter is in the range of the previously observed vesicles produced by prokaryotes (McBroom *et al*., 2006). The region of vesicle production requires special properties that are not yet completely understood (Kulp and Kuehn, 2010). These properties include a lack of membrane-peptidoglycan bonds and differences in the concentrations of certain proteins and lipids. In addition to the polarized cell flagellation, MMP cells could also be polarized in relation to the cell wall and protein and lipid distribution and create a microenvironment where vesicles can be produced in the membrane potion close to the acellular compartment.

Magnetosome chains are positioned parallel to each another in the periphery of both the sMMPs and eMMPs, which results in a net magnetic moment for the whole assemblage sufficient to efficiently transfer the torque from the magnetosome chains to the whole organism. In the 3D reconstruction, we observed that magnetosomes are distributed on both outer loops of the H-shaped cells, which face the external environment, suggesting that H-shaped cells could represent cells in the division process. Cell division constrictions between the magnetosome chains within the IECF-shaped cells were not observed, which supports the idea that the H-shaped cells are in fact dividing cells. This would suggest that the separation of the offspring initiates from the poles of the columnar cells. The cell division between sMMPs and eMMPs would occur along different axes, the shorter and longer cell axes respectively. The difference in the cell division processes could be related to the maintenance of the magnetic properties of the whole microorganism and the transfer of the magnetic polarity to the offspring in both situations without compromising the magnetotactic behaviour. The magnetic moment of the whole organism may not be optimized, as the magnetosomes in a chain are not coplanar or aligned in the same direction, reducing the net magnetic moment of the whole cell assemblage.

Because eMMPs produce mostly bullet-shaped magnetite and only occasionally irregular-shaped greigite magnetosomes (Chen *et al*., 2015), which is different from the irregular greigite magnetosomes synthesized by most sMMPs, information regarding the *mam* gene content and organization may contribute important data to elucidate the evolution of magnetotaxis. Greigite magnetosomes are found in most sMMPs (Wenter *et al*., 2009; Abreu *et al*., 2011) and are organized in several parallel chains. Chen *et al*. (2015) reported that most cells of *Ca*. M. rongchenensis produce only magnetite crystals, but some of them produce both magnetite and greigite magnetosomes. A single 16S rRNA coding gene sequence has been identified that indicates the homogenous phylotype of the *Ca*. M. rongchenensis in the sample and suggests that an environmental-physiological control of the greigite production may exist. In MTB capable of producing both magnetite and greigite magnetosomes (*Ca*. Magnetomorum strain HK-1, *Ca*. Desulfamplus magnetomortis BW-1), two sets of magnetosome gene clusters were detected, one thought to be responsible for greigite biomineralization whereas the other for magnetite magnetosomes biomineralization (Lefèvre *et al*., 2011). In most cases, the greigite-producing gene cluster is closely associated with the *mad* gene cluster (Lefèvre *et al*., 2013). Recently, functional evidence that *mad* genes are actually involved in biomineralization was reported (Rahn-Lee *et al*., 2015). However, in *Ca*. M. rongchenensis, no greigite-related *mam* gene cluster has been detected, suggesting plasticity in position for

the greigite-producing genes in this species. The function of *mad* genes in magnetosome formation is still poorly understood, but three *mad* genes (*mad1, mad2 and mad6*), which leads to non-magnetotactic or inefficient magnetotactic response in *Desulfovibrio magneticus* RS-1 mutants for these genes (Rahn-Lee *et al*., 2015) are present in *Ca*. M. rongchenensis. eMMPs from the coastal lagoon Lake Yuehu and Huiquan Bay (China) are capable of producing magnetite magnetosomes, either exclusively or together with greigite magnetosomes (Zhou *et al*., 2012; Zhang *et al*., 2014; Chen *et al*., 2015). Interestingly, single-cell genomics of the sMMP *Ca*. Magnetomorum strain HK-1 sampled from the same site (Wenter *et al*., 2009) showed two divergent magnetosome gene clusters, including a set of genes closely related to magnetite-producing genes. The 16S rRNA coding genes of *Ca*. Magnetomorum strain HK-1 (Kolinko *et al*., 2014) were 96.8% identical to those of *Ca*. Magnetomorum litorale (Wenter *et al*., 2009) and 99.3% identical to a sMMP that produces both magnetite and greigite magnetosomes (Zhang *et al*., 2014), indicating genetic variability or heterogeneity of MMP populations from the same site, possibly even beyond the species level.

Experimental procedures

Sampling

Water and sediment were collected from the Yellow Sea in Rongchen (37°21′N, 122°34′E) using plastic bottles and stored in the laboratory under dim light at room temperature. Magnetic enrichment was conducted according to Wolfe *et al*. (1987) to obtain enriched samples containing eMMPs, as previously described (Zhou *et al*., 2012; Chen *et al*., 2015).

Transmission electron microscopy

After the magnetic enrichment, eMMPs were fixed in 2.5% glutaraldehyde in sodium cacodylate buffer 0.1 M (pH 7.2) prepared in filtered sterilized seawater from the sampling site. After fixation, the cells were washed in sodium cacodylate buffer 0.1 M pH 7.2, post-fixed in buffered 1% OsO_4, dehydrated in an acetone series (30%, 50%, 70%, 90%, 100%), and embedded in Polybed 812 resin. For cytochemical staining, 2% tannic acid was added to the fixative solution. For thin-section transmission electron microscopy, ultrathin sections were obtained with a Leica ultramicrotome (Leica Microsystems, Wetzlar, Germany), stained with uranyl acetate and lead citrate and imaged with a FEI Morgagni TEM (FEI Company, Hillsboro, OR, USA) operating at 80 kV. Tomography data were obtained in Scanning Transmission Electron Microscopy (STEM) mode using a Tecnai G20 field emission gun microscope operating at 200 kV. Single tilt axis image series were acquired from −65° to 65° using the 'Satox scheme' for angle calculation steps at 64,000x direct magnification with automatic correction for focus and image shift variations using TIA software. Images were recorded with a Fishione high-angle annular dark field (HAADF) detector model M3000 with a camera length of 265 mm, resulting in a pixel size of 0.83 nm. Reconstruction and alignment of STEM tilt series were conducted using the IMOD package.

Scanning electron microscopy

After magnetic concentration, the *Ca*. M. rongchenensis were adhered to poly-L-lysine treated glass slides and fixed in 2.5% glutaraldehyde in 0.1 M sodium cacodylate buffer, pH 7.2, prepared in filtered sterilized seawater from the sampling site. After incubating for 1 h at room temperature, samples were washed in the same buffer, post-fixed in buffered 1% osmium tetroxide for 1 h, washed in the same buffer, dehydrated in an ethanol series (30%, 50%, 70%, 90%, 100%), critical-point dried with CO_2, sputtered with gold and imaged with a S3400N scanning electron microscope (Hitachi, Tokyo, Japan) operating at 25 kV.

Focused ion beam scanning electron microscopy (FIB-SEM) and 3D reconstruction

For FIB-SEM, samples were prepared according to the transmission electron microscopy protocol described above. Resin blocks containing the samples were attached to aluminium stubs and coated with a 30-nm thick Au layer. A Zeiss Auriga FIB/SEM XBeam system (Oberkochen, Germany) was used for ion milling and electron imaging. FIB milling was initially performed with a 30-keV Ga ion beam with a 2-nA current to polish and expose the sample to be milled and imaged. A trench that enabled viewing the cross-section of the MMPs was created in each sample. Then, a 600-pA beam was used to slice the sample at 30-nm intervals and create a slice-and-view image series of the samples. The final data acquisition was performed using a mixed electron signal consisting of 50% backscattered electrons and 50% secondary electrons in immersion lens mode (in-lens detector) with an accelerating voltage of 1.8 kV. Line averaging ($n = 30$) was used for noise reduction at an image resolution of 3073 × 2304, resulting in a total cycle time of approximately 1 min per image.

3D reconstruction models were obtained from FIB-SEM images using the IMOD software suite (Boulder Laboratory, University of Colorado, Boulder, CO, USA). Slice-and-view series were automatically aligned using the XfAlign IMOD software algorithm, and then a fine alignment was performed using MIDAS software. After image alignment and stacking, cell membrane, magnetosomes and granule profiles were manually traced in each slice using an Intuos 3 Wacom digital table (Vancouver, WA, USA) and used to render 3D models with 3DMOD software.

Genomic sequencing and analysis

The micromanipulation of single eMMPs was performed as previously described (Chen *et al*., 2015). Briefly, five to ten conspicuous eMMPs were transferred to 3 μl PBS from the REPLI-g Single Cell Kit (cat # 150343; QIAGEN, Germany). Subsequently, the PBS-suspended sample was frozen and thawed repeatedly, and the WGA reaction was carried out using the REPLI-g Single Cell Kit according to the manufacturer's instructions. The WGA reactions were carried out at

30°C for 6 h, yielding at least 1 μg DNA. Partial 16S rDNA was amplified from the WGA genomes using the bacteria-specific primers 27F and 1492R (Sangon Biotech, Shanghai, China). The resulting PCR products were cloned into the pMD18-T vector (Takara, Dalian, China) and transformed into competent Escherichia coli Top 10 cells. The clones were randomly selected for sequencing (Nanjing Genscript Biotechnology, Nanjing, China) to identify the individual single amplified genomes.

For genome sequencing, DNA libraries were generated and sequencing of 2 × 100 bp and 2 × 250 bp was performed with HiSeq 2500 and MiSeq sequencers (Illumina) respectively. After performing quality trimming and filtering, the passed single and paired reads were assembled using the SPAdes Genome Assembler. The putative magnetosome gene-containing contigs and flagellar genes were annotated using the automated annotation pipeline implemented in the MicroScope platform (Vallenet *et al.*, 2012) and were subsequently manually checked.

Acknowledgements

We thank Prof. Kildare Miranda for helping with the FIB-SEM data acquisition. We thank Centro Nacional de Biomagem (CENABIO)-UFRJ, Brazil for the use of their FIB/SEM microscopy facilities. This work was supported by grants NSFC 41330962, 41506147, 41506174 and 41606188 from the National Science Foundation of China and a grant for LIA-BioMNSL from the Centre National de la Recherche Scientifique. PL, FA and UL were funded by the Brazilian agencies CNPq, CAPES and FAPERJ. The funders had no role in the study design, data collection and interpretation, or the decision to submit the work for publication.

References

Altegoer, F., Schuhmacher, J., Pausch, P., and Bange, G. (2014) From molecular evolution to biobricks and synthetic modules: A lesson by the bacterial flagellum. *Biotechnol Genet Eng Rev* **30:** 49–64.

Abreu, F., Silva, K.T., Martins, J.L., and Lins, U. (2006) Cell viability in multicellular magnetotactic prokaryotes. *Int. Microbiol* **9:** 267–272.

Abreu, F., Martins, J.L., Silveira, T.S., Keim, C.N., De Barros, H.G.P.L., Filho, F.J.G., and Lins, U. (2007) 'Candidatus Magnetoglobus multicellularis', a multicellular, magnetotactic prokaryote from a hypersaline environment. *Int J Syst Evol Microbiol* **57:** 1318–1322.

Abreu, F., Cantão, M.E., Nicolás, M.F., Marisa, F., Barcellos, F.G., Morillo, V.,, *et al.* (2011) Common ancestry of iron oxide- and iron-sulfide-based biomineralization in magnetotactic bacteria. *ISME J* **5:** 1634–1640.

Abreu, F., Silva, K.T., Leão, P., Guedes, I.A., Keim, C.N., Farina, M., and Lins, U. (2013) Cell adhesion, multicellular morphology, and magnetosome distribution in the multicellular magnetotactic prokaryote Candidatus Magnetoglobus multicellularis. *Microsc Microanal* **19:** 535–543.

Abreu, F., Morillo, V., Nascimento, F.F., Ribeiro, C.W., Catao, M.E., Ciapina, L.P., *et al.* (2014) Deciphering unusual uncultured magnetotactic multicellular prokaryotes through genomics. *ISME J* **8:** 1055–1068.

Bazylinski, D.A., and Frankel, R.B. (2004) Magnetosome formation in prokaryotes. *Nat Rev Microbiol* **2:** 217–230.

Berleman, J., and Auer, M. (2013) The role of bacterial outer membrane vesicles for intra- and interspecies delivery. *Environ Microbiol* **15:** 347–354.

Bobik, T.A., Havemann, G.D., Busch, R.J., Williams, D.S., and Aldrich, H.C. (1999) The propanediol utilization (pdu) operon of *Salmonella enterica* serovar Typhimurium LT2 includes genes necessary for the formation of polyhedral organelles involved in coenzyme B12-dependent 1,2-propanediol degradation. *J Bacteriol* **181:** 5967–5975.

Briegel, A., Ladinsky, M.S., Oikonomou, C., Jones, C.W., Harris, M.J., Fowler, D.J., *et al.* (2014) Structure of bacterial cytoplasmic chemoreceptor arrays and implications for chemotactic signaling. *eLife* **3:** e02151. doi: 10.7554/eLife.02151

Byrne, M.E., Ball, D.A., Guerquin-Kern, J.-L., Rouillere, I., Wuc, T.-D., Downing, K.H., *et al.* (2010) *Desulfovibrio magneticus* RS-1 contains an iron- and phosphorus-rich organelle distinct from its bullet-shaped magnetosomes. *Proc Natl Acad Sci USA* **107:** 12263–12268.

Chen, S., Beeby, M., Murphy, G.E., Leadbetter, J.R., Hendrixson, D.R., Briegel, A., *et al.* (2011) Structural diversity of bacterial flagellar motors. *EMBO J* **30:** 2972–2981.

Chen, Y.R., Zhang, R., Du, H.J., Pan, H.M., Zhang, W.Y., Zhou, K., *et al.* (2015) A novel species of ellipsoidal multicellular magnetotactic prokaryotes from Lake Yuehu in China. *Environ Microbiol* **17:** 637–647.

Chen, Y.R., Zhang, W.Y., Zhou, K., Pan, H.M., Du, H.J., Xu, C., *et al.* (2016) Novel species and expanded distribution of ellipsoidal multicellular magnetotactic prokaryotes. *Environ Microbiol Rep* **8:** 218–226.

Farina, M., Lins de Barros, H.G.P., Esquivel, D.M.S., and Danon, J. (1983) Ultrastructure of a magnetotactic microorganism. *Biol Cell* **48:** 85–88.

Frankel, R.B., Bazylinski, D.A., Johnson, M.S., and Taylor, B. (1997) Magneto-Aerotaxis in Marine Coccoid Bacteria. *Biophys J* **73:** 994–1000.

Ji, B., Zhang, S.D., Arnoux, P., Rouy, Z., Alberto, F., Philippe, N., *et al.* (2014) Comparative genomic analysis provides insights into the evolution and niche adaptation of marine Magnetospira sp. QH-2 strain. *Environ Microbiol* **16:** 525–544.

Keim, C.N., Abreu, F., Lins, U., Barros, H.G.L., and Farina, M. (2004a) Cell organization and ultrastructure of a magnetotactic multicellular organism. *J Struct Biol* **145:** 254–262.

Keim, C., Martins, J.L., Abreu, F., Rosado, A.S., Lins de Barros, H.G.P., Borojevic, R., *et al.* (2004b) Multicellular life cycle of magnetotactic prokaryotes. *FEMS Microbiol Lett* **240:** 203–208.

Kolinko, I., Lohße, A., Borg, S., Raschdorf, O., Jogler, C., Tu, Q., *et al.* (2014) Biosynthesis of magnetic nanostructures in a foreign organism by transfer of bacterial magnetosome gene clusters. *Nat Nanotechnol* **9:** 193–197.

Kulp, A., and Kuehn, M.J. (2010) Biological functions and biogenesis of secreted bacterial outer membrane vesicles. *Annu Rev Microbiol* **64:** 163–184.

Rahn-Lee, L., Byrne, M.E., Zhang, M., Le Sage, D., Glenn, D.R., Milbourne, T., *et al.* (2015) A genetic strategy for probing the functional diversity of magnetosome formation. *PLoS Genet* **11:** e1004811.

Lefèvre, C., Bernadac, A., Pradel, N., Wu, L., Yu-Zhang, K., Xiao, T., *et al*. (2007) Characterization of Mediterranean magnetotactic bacteria. *J Ocean Univ China* **6:** 355–359.

Lefèvre, C., Abreu, F., Lins, U., and Bazylinski, D. (2010) Non-magnetotactic multicellular prokaryotes from low saline, nonmarine aquatic environments and their unusual negative phototactic behavior. *Appl Environ Microbiol* **76:** 3220–3227.

Lefèvre, C.T., Menguy, N., Abreu, F., Lins, U., Pósfai, M., Prozorov, T., *et al*. (2011) A cultured greigite-producing magnetotactic bacterium in a novel group of sulfate-reducing bacteria. *Science* **334:** 1720–1723.

Lefèvre, C.T., Trubitsyn, D., Abreu, F., Kolinko, S., Jogler, C., De Almeida, L.G.P., *et al*. (2013) Comparative genomic analysis of magnetotactic bacteria from the *Deltaproteobacteria* provides new insights into magnetite and greigite magnetosome genes required for magnetotaxis. *Environ Microbiol* **15:** 2712–2735.

Lins, U., Keim, C.N., Evans, F., Buseck, P.R., and Farina, M. (2007) Magnetite (Fe_3O_4) and greigite (Fe_3S_4) crystals in multicellular magnetotactic prokaryotes. *Geomicrobiol J* **24:** 43–50.

Lin, W., Benzerara, K., Faivre, D., and Pan, Y. (2014) Intracellular biomineralization in bacteria. *Front Microbiol* **5:** 293. doi: 10.3389/fmicb.2014.00293.

McBroom, A.J., Johnson, A.P., Vemulapalli, S., and Kuehn, M.J. (2006) Outer membrane vesicle production by *Escherichia coli* is independent of membrane instability. *J Bacteriol* **188:** 5385–5392.

Posfai, M., Buseck, P.R., Bazylinski, D.A., and Franke, R.B. (1998) Iron sulfides from magnetotactic bacteria: structure, composition, and phase transitions. *Am Mineral* **83:** 1469–1481.

Rae, B.D., Long, B.M., Badger, M.R., and Dean Price, G. (2013) Functions, compositions, and evolution of the two types of carboxysomes: polyhedral microcompartments that facilitate CO_2 fixation in cyanobacteria and some proteobacteria. *Microbiol Mol Biol Rev* **77:** 357–379.

Rodgers, F.G., Blakemore, R.P., Blakemore, N.A., Frankel, R.B., Bazylinski, D.A., Maratea, D., and Rodgers, C. (1990) Intercellular structure in a many-celled magnetotactic prokaryote. *Arch Microbiol* **154:** 18–22.

Schuhmacher, J.S., Thormann, K.M., and Bange, G. (2015) How bacteria maintain location and number of flagella? *FEMS Microbiol Rev* **39:** 812–822.

Silva, K.T., Abreu, F., Almeida, F.P., Keim, C.N., Farina, M., and Lins, U. (2007) The flagellar apparatus in south-seeking many-celled magnetotactic prokaryotes. *Microsc Res Tech* **70:** 10–17.

Simmons, S.L., and Edwards, K.J. (2007) Unexpected diversity in populations of the many-celled magnetotactic prokaryote. *Environ Microbiol* **9:** 206–215.

Vallenet, D., Belda, E., Calteau, A., Cruveiller, S., Engelen, S., and Lajus, A., *et al*. (2012) MicroScope—an integrated microbial resource for the curation and comparative analysis of genomic and metabolic data [J]. *Nucleic Acid Re* gks1194.

Wenter, R., Wanner, G., Schüler, D., and Overmann, J. (2009) Ultrastructure, tactic behaviour and potential for sulfate reduction of a novel multicellular magnetotactic prokaryote from North Sea sediments. *Environ Microbiol* **11:** 1493–1505.

Winklhofer, M., Abraçado, L.G., Davila, A.F., Keim, C.N., and Lins de Barros, H.G.P. (2007) Magnetic optimization in a multicellular magnetotactic organism. *Biophys J* **92:** 661–670.

Wolfe, R.S., Thauer, R.K., and Pfennig, N. (1987) A "capillary racetrack" method for isolation of magnetotactic bacteria. *FEMS Microbiol Lett* **45:** 31–35.

Zhang, R., Chen, Y.R., Du, H.J., Zhang, W.Y., Pan, H.M., Xiao, T., and Wu, L.F. (2014) Characterization and phylogenetic identification of a species of spherical multicellular magnetotactic prokaryotes that produces both magnetite and greigite crystals. *Res Microbiol* **161:** 481–489.

Zhou, K., Zhang, W.Y., Yu-Zhang, K., Pan, H.M., Zhang, S.D., Zhang, W.J., *et al*. (2012) A novel genus of multicellular magnetotactic prokaryotes from the Yellow Sea. *Environ Microbiol* **14:** 405–413.

Zhou, K., Zhang, W.Y., Pan, H.M., Zhang, S.D., Li, J.H., Yue, H.D., Xiao, T., and Wu, L.F. (2013). Adaptation of spherical multicellular magnetotactic prokaryotes to the geochemically variable habitat of an intertidal zone. *Environment Microbiol* **15:** 1595–1605.

Supporting information

Additional Supporting Information may be found in the online version of this article at the publisher's website:

Table S1. Comparison of putative magnetosome proteins identified from the MAI contig (GenBank Accession number KY084568) of draft genome of Candidatus Magnetananas rongchenensis RPA with those of all MTB.